Geochemical Interactions of Plutonium with Opalinus Clay Studied by Spatially Resolved Synchrotron Radiation Techniques

Kaplan, U.; Amayri, S.; Drebert, J.; Rossberg, A.; Grolimund, D.; Reich, T.;

Originally published:

May 2017

Environmental Science & Technology 51(2017), 7892-7902

DOI: https://doi.org/10.1021/acs.est.6b06528

Geochemical Interactions of Plutonium with Opalinus Clay Studied by Spatially Resolved Synchrotron Radiation Techniques

Journal:	*Environmental Science & Technology*
Manuscript ID	es-2016-06528j.R2
Manuscript Type:	Article
Date Submitted by the Author:	21-May-2017
Complete List of Authors:	Kaplan, Ugras; Karlsruhe Institute of Technology (KIT), Institute for Nuclear Waste Disposal (INE); Johannes Gutenberg-Universität, Institut für Kernchemie Amayri, Samer; Johannes Gutenberg-Universität, Institut für Kernchemie Drebert, Jakob; Johannes Gutenberg-Universität, Institute of Nuclear Chemistry Rossberg, Andre; Forschungszentrum Dresden-Rossendorf, Institute of Radiochemistry Grolimund, Daniel; Paul Scherrer Institute, Swiss Light Source Reich, Tobias; Institut fur Kernchemie, Johannes Gutenberg Universitat Mainz

Geochemical Interactions of Plutonium with Opalinus Clay Studied by Spatially Resolved Synchrotron Radiation Techniques

Ugras Kaplan[1], Samer Amayri[1], Jakob Drebert[1], Andre Rossberg[2], Daniel Grolimund[3,*], Tobias Reich[1,*]

[1] Johannes Gutenberg-Universität Mainz, Institute of Nuclear Chemistry, Fritz-Strassmann-Weg 2, 55128 Mainz, Germany

[2] Helmholtz-Zentrum Dresden-Rossendorf (HZDR), Institute of Resource Ecology, Bautzner Landstraße 400, 01328 Dresden, Germany.

[3] Paul Scherrer Institute, Swiss Light Source, microXAS Beamline Project, 5232 Villigen PSI, Switzerland

* Corresponding authors:

treich@uni-mainz.de (+49 6131 3925250); daniel.grolimund@psi.ch (+41 56 310 4782)

Abstract

Plutonium plays an important role within nuclear waste materials because of its long half-life and high radiotoxicity. The aim of this study was to investigate with high spatial resolution the reactivity of the more oxidized forms of Pu(V,VI) within Opalinus Clay (OPA) rock, a heterogeneous, natural argillaceous rock considered as potential repository host. A combination of synchrotron based X-ray microprobe and bulk techniques were used to study the spatial distribution and molecular speciation of Pu within OPA after diffusion and sorption processes. Microscopic chemical images revealed a pronounced impact of geochemical heterogeneities concerning the reactivity of the natural barrier material. Spatially resolved X-ray absorption spectroscopy documented a reduction of the highly soluble Pu(V,VI) to the less mobile Pu(IV) within the argillaceous rock material, while bulk investigations showed second-shell scattering contributions, indicating an inner-sphere sorption of Pu on OPA components. Micro-diffraction imaging identified the clay mineral kaolinite to play a key role in the immobilization of the reduced Pu.

The findings provide strong evidence that reduction and immobilization do not occur as linked processes on a single reactive phase but as decoupled, subsequent and spatially separated reactions involving different phases of the OPA.

Keywords: Plutonium, Opalinus Clay, micro-XANES, micro-XRD, micro-XRF, XANES/EXAFS, speciation, sorption, migration, synchrotron microprobe techniques

1. Introduction

The breach of the first containment and the resulting release of radionuclides out of the storage canisters and subsequent migration through the enclosing multi-barrier system corresponds to an accepted and considered incident within safety assessments of waste repositories [1, 2]. To assess the potential risk of impairing host rock formations, neighboring

aquifers and finally the biosphere, the mobility and immobilization behavior of radionuclides in multi-barrier systems have to be investigated. Beside other actinides, plutonium (Pu) will be a major contributor to the radiotoxicity of high-level nuclear waste after a storage time of more than 1,000 years due to the long half-lives and radiotoxicity of its isotopes ^{239}Pu and ^{240}Pu [3-7].

Considering the chemical properties of Pu, this element reveals a complicated redox behavior as it can exist in aqueous solution in different oxidation states (typically III-VI), depending on the chemical conditions such as pH, Eh, and ionic strength. Up to three oxidation states of Pu can coexist in natural waters. The oxidation states V and VI have low tendency for hydrolysis, precipitation, and sorption on natural minerals [8-10]. Accordingly, related species exhibit a pronounced mobility in subsurface systems. In contrast, the reduced oxidation states Pu(III) and Pu(IV) prevail as solids with low solubility and show a high affinity for mineral surfaces (strong adsorption or surface precipitations) resulting in a considerable retardation of the Pu spreading. Consequently, the migration behavior of Pu in the environment depends strongly on its oxidation state and related pore water chemistry (pH, redox potential, ionic strength, electrolyte composition, and complexing agents) but also on the geochemical characteristics of the host rock material, e.g., its mineralogy [11].

Based on the typical initial waste forms and the reducing conditions in a nuclear waste repository, plutonium is expected to be present initially in its more reduced form of +IV in the repository [12, 13]. However, over time waters with increasing levels of dissolved oxygen may infiltrate the repository, potentially oxidizing Pu to its more mobile forms of +V and +VI. Accordingly, due to their increased mobility in subsurface systems and the resulting increased environmental risk, the present study focuses on the higher oxidized forms of Pu.

Based on their high cation retardation potential and advantageous physical properties – e.g. the self-sealing due to swelling – argillaceous rocks are considered as a potential host rock formation for the construction of high-level nuclear waste repositories in several European

73 countries [4,5,6,7]. In this study Opalinus Clay (OPA) rock, which is present in southern
74 Germany and Switzerland, was used as a natural reference barrier material. Predominantly,
75 OPA consists of different types of clay minerals, in particular illite, illite/smectite mixed
76 layers, and kaolinite, with minor components such as calcite, quartz, and the Fe(II)-bearing
77 minerals pyrite and siderite (see Supporting Information (SI). Regarding the potential
78 application as host rock for a nuclear waste repository, OPA rock has favorable properties
79 such as low hydraulic permeability as well as stable geochemical conditions and mechanical
80 properties [14]. Several geological studies document that the present geological settings can be
81 considered as being unchanged for several millions of years [15].
82
83 In compacted clay barrier systems, diffusion – potentially retarded by sorption and/or
84 precipitation – corresponds to the predominant transport phenomena determining the
85 spreading of radionuclides [16] (while in advection dominated systems with larger transport
86 pores colloid facilitated transport could become an additional relevant transport vector [17, 18]).
87 Accordingly, the investigation of reactions occurring at the solid-solution interface is most
88 fundamental towards an in-depth understanding of the retarded spreading of Pu in compacted
89 reactive barrier systems. This topic received indeed considerable attention in the past.
90 However, the vast majority of the corresponding investigations represent macroscopic scale
91 studies employing a single, well defined solid, commonly pure or even synthetic mineral
92 phase.
93
94 Several studies have been performed to investigate the interaction of Pu with pure clay
95 minerals (e.g., kaolinite [19, 20], illite [21], or Na-montmorillonite [22, 23]). Pu sorption onto
96 oxide/hydroxide mineral surfaces such as goethite and hematite [24, 25], manganite and
97 hausmannite [26], or magnetite [27], to sulfides (e.g., mackinawite [27]), or onto carbonates (e.g.,
98 calcite [28] or chukanovite [27]) was also examined. These studies showed that the sorption

behavior of Pu depends indeed significantly on its oxidation state, the prevailing pH conditions, ambient CO_2 partial pressure, and the type of mineral surfaces present. For example, in the study of Sanchez et al. [24], Pu(V) was reduced to Pu(IV) by a 'surface mediated' process and immobilized on the goethite surface (although without identification of the corresponding electron donor). Ionic strength variations in the range between 0.03 M and 3.0 M did not influence the sorption of Pu(IV), indicative of a covalent bonding of Pu(IV) to the goethite. The sorption of Pu was further shown to decrease in carbonate media due to the formation of aqueous Pu-carbonate complexes documenting the importance of ligands (or pore water chemistry in general) in the context of subsurface Pu mobility.

Only a limited number of studies addresses the environmental reactivity of Pu(V) and Pu(VI) within complex natural barrier materials. Amayri et al. [29] studied the sorption of Pu and other actinides on OPA material by batch sorption experiments. This study showed that the affinity for the solid surfaces depends strongly on the oxidation state of the actinides. The determined sorption affinities for the tri- and tetravalent actinides such as Pu(III/IV) were almost 3 orders of magnitude stronger compared to actinide species of oxidation states +V and +VI. Compared to U(VI), that was stable during the experiments of Amayri et al., Pu(VI) expressed a more than 250 times higher uptake by OPA, a peculiarity construed by the authors as indication for a change in oxidation state of Pu(VI) during the sorption process. For the interaction of Pu(V) with bentonite, the time-dependent investigations of Begg et al. [30] revealed a slow, continuous uptake of Pu(V) over 300 days. Supported by indirect evidences, the authors attributed this observation to a slow reduction of Pu(V) on clay surfaces. Hixon et al. [31] observed 'surface mediated reduction' in case of Pu(V) reacting with Savannah River Site sediment material. Interestingly, Pu(V) was the dominant aqueous species, while the Pu reacted with the solid phase was determined to be Pu(IV).

124 While several field observations point to subsurface migration of Pu (see e.g., 2013 review by
125 Kersting [32]), controlled laboratory-based or field-scale reactive transport studies investigating
126 the spreading of Pu in subsurface porous media are scarce. In an early study, Ashida et al. [33]
127 recorded and modelled diffusion profiles of Pu released by waste glass corrosion in
128 compacted bentonite. In a series of transport studies, Kaplan and co-workers [34, 35] documented
129 the importance of redox processes for the mobility of Pu in porous media based on Savannah
130 River Site sediment material.
131
132 While macroscopic investigations provide valuable (empirical) information regarding the
133 composite behavior of a complex system, only limited information can be obtained
134 concerning individual processes and mechanisms contributing to the final reactivity and
135 corresponding evolution of a given system. However, in view of reliable safety assessments it
136 is important to derive a mechanistic, process-based understanding. Consequently, it is
137 mandatory to examine the interaction of Pu with geo-materials, additionally, on a microscopic
138 scale as well as on a molecular level. In the literature only limited information can be found
139 concerning the interaction of Pu with compacted barrier materials or their key components
140 such as clay minerals on a molecular level. Briefly, Reich et al. [36] applied X-ray absorption
141 fine structure (XAFS) spectroscopy to investigate the speciation of Pu after sorption on
142 kaolinite in dependence on several experimental parameters such as Pu oxidation state (+III
143 and +IV), ambient CO_2 partial pressure, and pH. The result showed an inner-sphere sorption
144 of polynuclear Pu(IV) species on the kaolinite surface independent of the initial oxidation
145 state[36]. Kirsch et al. used Pu L_{III}-edge XANES (X-ray absorption near edge structure) and
146 EXAFS (extended X-ray absorption fine structure) spectroscopy to investigate the reaction
147 between aqueous Pu(III) or Pu(V) and different Fe(II)-bearing minerals (magnetite,
148 mackinawite, and chukanovite), which are formed as corrosion products of nuclear waste steel
149 containers under anoxic conditions. Pu(V) was reduced in the presence of all three minerals.

In the presence of mackinawite and chukanovite solid $Pu^{IV}O_2$ phases were formed. Additionally, in the case of chukanovite and magnetite a significant fraction of plutonium was further reduced to Pu(III). In both cases, the observed spectroscopic signatures related to Pu(III) point to sorption complexes on the iron mineral phases rather than the precipitation of a Pu(III) solid phase [27]. Generally, reduced manganese and iron species present in different minerals have been reported to reduce Pu(V) and Pu(VI) to Pu(IV) [25, 26].

Applying molecular-level techniques to complex natural systems, Kaplan et al. investigated the mobility of Pu in different oxidation states (+III, +IV, +V, +VI) in red clay over a period of 2 - 11 years. Their studies showed that Pu mobility was influenced by both, the initial Pu oxidation state and occurring oxidation state transformations of Pu after coming in contact with the sediment. Using XANES spectroscopy and solvent extraction methods they found that the Pu oxidation state distribution in the sediments after 11 years was dominated by Pu(IV) and Pu(III) with minor amounts of Pu(V) and Pu(VI) as well as polymerized, neutral Pu species [31, 34].

A combination of synchrotron-based micro-analytical techniques can be used to gain a molecular-level understanding of the migration processes of actinides in heterogeneous materials and to detect the spatial distribution of immobilized actinides and other co-associated elements within geologic subsurface porous media. Duff et al. studied the sorption of dissolved Pu(V) on a natural zeolitic tuff [37, 38]. Synchrotron-based micro-XRF showed that Pu is predominantly associated with manganese oxides and smectites but not with iron oxides. In-situ micro-XANES measurements on two highly enriched regions of Pu indicated that the average oxidation state of sorbed Pu was Pu(V) in one region and Pu(VI) in the other. Denecke et al. used micro-focused synchrotron radiation techniques to study a natural, uranium-rich tertiary sediment collected from Ruprechtov (Czech Republic). This study

evidenced AsFeS coating on framboid Fe nodules in the sediment to reduce the highly mobile aqueous U(VI) to less-soluble U(IV), thus immobilizing the uranium in the sediment [39]. Recently, Fröhlich et al. [40] used spatially resolved micro-XRF, X-ray absorption spectroscopy (micro-XAS), and micro-XRD to determine the reactivity of Np in natural Opalinus Clay. The results showed that Np(V) was reduced to Np(IV) by an Fe(II)-containing mineral identified by micro-XRD as pyrite.

Kaplan et al. [34] employed synchrotron-based micro-XRF imaging and micro-XANES to study lysimeter sediments amended with different Pu species. This study showed pronounced hotspots with high local Pu concentration. Interestingly, despite the documented reduction of Pu over the course of the long-term experiments, the distribution of Pu in the sediments was not correlated to Mn or Fe.

Until now, no comparable studies with high spatial resolution can be found in the literature investigating the reactivity of Pu within a natural reactive barrier material such as OPA. Therefore, our aim was to improve the understanding of the geochemical interaction of Pu with OPA on a molecular level. The focus was on the determination of the speciation of Pu immobilized by OPA during diffusion processes and to identify the most reactive constituents of the reactive barrier. Investigations with high spatial resolution by combining different synchrotron-based micro-analytical techniques were employed to unravel the complexity of the heterogeneous geological material. The spatial distribution of Pu and its correlation with other elements contained in OPA (i.e., Ca, Fe, Mn) were determined by micro-XRF mapping. The oxidation state and molecular structure of the sorbed Pu species were analyzed by micro-XAS spectroscopy, while the reactive crystalline constituents of the heterogeneous OPA were identified by micro-XRD. These microscopic investigations were complemented by Pu L_{III}-edge EXAFS spectroscopy measurements of Pu reacted with powdered OPA material.

Such complementary, multimodal investigations are essential to decipher the fundamental reactive processes occurring in natural and engineered repository barriers and contribute

202 therefore in a fundamental manner to the save disposal and long-term storage of hazardous
203 radioactive materials.
204
205
206 **2. Materials and methods**
207 **2.1 Materials**
208 Details regarding the employed Opalinus Clay rock material and the preparation of the Pu(VI)
209 stock solutions can be found in the SI.
210
211 **2.2. Sample preparation**
212 **2.2.1. Sorption on OPA powder sample**

213 For EXAFS measurements, two powder samples were prepared based on batch sorption
214 experiments. The sorption of Pu(IV) and Pu(VI) on OPA powder (Table S1) was investigated
215 using synthetic OPA pore water [41] under anaerobic conditions (Ar-atmosphere). The sorption
216 experiments were carried out in 50 mL centrifuge tubes (Beckman Coulter, USA) with a total
217 solution volume of 40 mL. In each tube, OPA powder (240 mg) was preconditioned for
218 72 hours with OPA pore water. After the preconditioning, the OPA suspensions were spiked
219 with Pu(IV) or Pu(VI) from the ^{239}Pu stock solutions resulting in initial Pu concentrations of
220 10 µM and 20 µM, respectively. During the equilibration time of 60 hours, the pH of the
221 samples was adjusted to the desired value of about 7.6 by adding small amounts of NaOH or
222 $HClO_4$ stock solutions, respectively. The pH measurements were performed using a pH meter
223 (inoLab pH/Cond 720, WTW, Germany) equipped with a pH electrode (blue line 16 pH, SI
224 Analytics GmbH, Germany). After equilibration, the suspension was separated by a two-step
225 centrifugation procedure, first at 4025 g for 5 min (SIGMA 3K30, Sigma Laborzentrifugen
226 GmbH, Germany), followed by 108'000 g for 1 h (Avanti J-30I, Beckman Coulter, USA).
227 The Pu uptake was calculated based on the difference between initial and equilibrium Pu

concentrations in solution and the known solid-to-liquid ratio (6 g/L). The aqueous Pu concentrations were determined by liquid scintillation counting (LSC) using a home built scintillation counter measuring 1 mL sample in 10 mL scintillation cocktail Ultima Gold™ XR (PerkinElmer, USA). Chemical conditions observed at the end of the equilibration period are reported in Table S2. The powder of each sample was dried under anaerobic conditions for 3 days at 26 °C, grinded, loaded into a special polyethylene sample holder, sealed, and transported to the European Synchrotron Radiation Facility (ESRF) either in an anaerobic jar (Schuett-biotec GmbH, Germany) purged with argon (for Pu(VI) sample) or in a special dewar filled with liquid nitrogen (Voyageur 12, AIR LIQUIDE Deutschland GmbH, Germany), in which the sample of Pu(IV) was kept at cryogenic conditions until the measurement.

2.2.2. Sorption on intact OPA thin section

A thin section of OPA on a high-purity quartz glass slide (Heraeus Holding GmbH, Germany) was prepared at the Max-Planck-Institute for Chemistry, Mainz. This thin section had a thickness of ~25 µm and a total surface of approximately 1 cm^2. A 20 µM ^{242}Pu solution (Millipore water, pH adjusted to 7.6, spiked with ^{242}Pu(VI) stock solution) was contacted with the thin section surface using an in-house engineered sorption cell. Pu(V) can be expected to be the predominant Pu species in the supernatant reservoir over the course of the experiment (see also SI). After a contact time of five days under ambient air conditions, the supernatant solution was removed. The final Pu concentration in the supernatant was measured by LSC and the amount of Pu sorbed per surface area OPA was determined. The surface area of the thin section contacted with Pu was sealed with Kapton foil immediately after removal of the

253 solution phase, loaded into a polyethylene sample holder and transported to the Swiss Light
254 Source (SLS).
255
256 **2.2.3. Diffusion in OPA core**
257 One sample was produced by an in-diffusion experiment. A cylinder (25×11 mm [diameter ×
258 height]) of aerobic OPA was placed in a stainless steel diffusion cell [42] and preconditioned
259 with synthetic OPA pore water [41] (pH 7.6, I = 0.4 M, however without Sr^{2+} to avoid spectral
260 interferences between Sr (K_α at 14165 eV) and Pu (L_α at 14278 eV, see below)) for 6 weeks.
261 The orientation of the clay rock core was chosen such that the direction of diffusion was
262 parallel to the bedding planes of the clay. Prior to the in-diffusion of Pu, tritiated water (HTO)
263 was used to characterize the OPA bore core by determining its porosity (ε) and the diffusion
264 coefficient of water (D_e) by means of a through-diffusion experiment. The obtained D_e value
265 agrees well with literature values [43, 44], while the porosity of the used OPA bore core is
266 slightly higher (Table S3).
267 For a duration of one month, ^{242}Pu was diffusing from a reservoir into the OPA rock sample.
268 Initial reservoir conditions were 20 µM ^{242}Pu(VI) in OPA reference pore water with a pH of
269 7.6 and a solution reservoir volume of 151 mL. However, Pu(V) can be expected to be the
270 predominant Pu species in the supernatant reservoir over the course of the experiment (see
271 also SI). The final Pu concentration in the reservoir was analyzed using LSC. About 90 % of
272 the initial Pu diffused into the OPA core resulting in a final concentration of $[^{242}Pu]_{final}$ =
273 1.9 µM. The clay core was removed from the cell, dried at ambient conditions and cut into
274 small pieces. These subsamples were placed in dedicated sample holders, sealed with Kapton
275 foil, and transported to the Swiss Light Source (SLS).
276
277 A summary of the experimental methods, prepared samples, and related chemical conditions
278 is provided in Tables S1 and S2.

279

280

281 **2.3. Measurements and data evaluation**

282 **2.3.1. XANES and EXAFS**

283 The Pu L_{III}-edge (18057 eV) EXAFS data of the powder samples were recorded at ROBL
284 (Rossendorf Beamline, ESRF, Grenoble, France). Data were measured in fluorescence mode
285 using a 13-element Ge-detector (Canberra, USA). The X-ray beam was monochromatized by
286 a Si(111) double-crystal monochromator. Higher order harmonic radiation was suppressed by
287 two focusing mirrors. The sample was measured at 15 K using a He cryostat (CryoVac
288 GmbH, Germany). The energy calibration was carried out by parallel measurement of a Zr
289 foil (Zr K-edge at 17998 eV). Further details regarding EXAFS measurements at ROBL can
290 be found in [45]. The EXAFS analysis was performed with the programs ATHENA [46] and
291 EXAFSPAK [47]. Theoretical scattering phases and amplitudes were calculated with FEFF8.20
292 [48] based on a hypothetical molecular cluster derived from the crystal structures of thorium
293 iron phosphide oxide ($Th_4Fe_{17}P_{10}O_{1-x}$) [49], where Th and P were replaced by Pu and Si/Al to
294 model possible Pu-Si/Al and Pu-Fe interactions with the OPA surface. The average oxidation
295 state of Pu in the bulk EXAFS samples was determined by fitting the XANES region between
296 18050 and 18130 eV by a linear combination of standard spectra (Pu(III) [50], Pu(IV) [51], Pu(V)
297 [52], and Pu(VI) [53]).

298

299

300 **2.3.2. micro-XANES, micro-XRF, and micro-XRD**

301 All spatially resolved measurements were performed at the microXAS beamline at the SLS.
302 The beamline is equipped with a Kirkpatrick-Baez mirror based microfocusing system and a
303 double-crystal monochromator with three different crystal pairs (Si(111), Si(311), and
304 Ge(111)). In our experiment only the Si(111) crystals were used. The energy calibration was

performed using a Zr foil. The X-ray fluorescence was measured using a single-element Si-drift detector (KETEK GmbH, Germany). To resolve the potential spectral interference between Pu (L_α at 14278 eV) and geogenic Sr (K_α at 14165 eV), the local Pu concentrations were reconstructed from the difference of two micro-XRF maps, recorded below (17900 eV) and above (18070 eV) the Pu L_{III}-edge (see also ref. [37]). Overview maps were recorded with pixel resolutions between 10 and 20 µm. High-resolution mappings were collected with 1 to 5 µm pixel resolution using a focused X-ray beam size of 3 × 1.5 μm^2 (h × v). Micro-XRF maps were processed and analyzed using facility provided MATLAB scripts.

X-ray diffraction images were recorded with a 100K Pilatus detector (DECTRIS Ltd., Switzerland). The Pilatus XRD detector geometry was calibrated by measuring reference powder pattern of α-Al_2O_3. Each area selected for micro-XRD imaging had a size of 11 × 11 μm^2 and was generally recorded with a step size of 1 µm resulting in 121 patterns. Particular features have been measured in more detail using a pixel resolution of 0.5 µm. Micro-XRD data were analyzed using the XRDUA software package [54].

Pu L_{III}-edge micro-XANES investigations were performed on several Pu hot spots in fluorescence mode with an angle of 45 degrees between incoming X-ray beam and fluorescence detector. In each location multiple scans were collected. Background and energy corrections of the spectra were performed with the program ATHENA [46]. Linear combination fitting analysis based on reference spectra (see above) was used to determine the fractions of different Pu oxidation states in the measured hot spots.

3. Results and Discussion

3.1. XANES and EXAFS measurements of OPA powder sample

XANES and EXAFS data obtained for Pu(V,VI) immobilized by powdered Opalinus Clay material are shown in Figure 1 (top) and Figure 2, respectively. Such spectroscopic data provide molecular-level information regarding the chemical speciation of Pu immobilized either as sorbed species at the solid-liquid interface or as secondary precipitate. However, such ('bulk') measurements provide system averaged information – an important point to consider, in particular in case of heterogeneous systems such as the OPA material.

The XANES spectrum depicted in Figure 1 (top) yields a Pu L_{III}-edge position of 18068 ± 1 eV. This value coincides with the Pu L_{III}-edge energy position measured for the Pu(IV) aquo ion [55, 56]. A more detailed analysis employing linear combination fitting analysis (LCFA) based on reference spectra shows indeed that at least two thirds of the initial Pu(VI) were reduced to Pu(IV) (68 ± 2 %), while one fifth was detected to be Pu(V) (20 ± 5 %). The original oxidation state of Pu(VI) was detected only in trace levels (12 ± 6 %). Consequently, electron transfer reactions play an important role regarding the sequestration of Pu(VI) by OPA.

The Pu L_{III}-edge, k^3-weighted EXAFS spectrum of the same sample is presented in Figure 2 together with the corresponding Fourier transform magnitude. In addition to the experimental data, the fitting results of two models, each of them considering two coordination spheres, are also included in the figure. The Fourier transform shows two main peaks. The first coordination shell is best described within these two fits by 6.8 or 7.1 oxygen atoms with an average Pu-O distance of 2.32 and 2.31 Å, respectively. The second peak can be modeled by various approaches involving different backscattering atoms, including Si, Al, or Fe for example. One first appropriate fit is obtained using a combination of Pu-Si/Al (at 3.10 Å) and

Pu-Fe/Mn (at 3.43 Å) scattering pairs in the second coordination shell (green line), while the second fit (red line) is based on two distinct sub-shells considering only Si/Al in the second shell (at 3.15Å and at 3.64 Å). Table S4 lists a summary of the molecular structure information obtained by the EXAFS fitting. Due to the restricted accessible k-range (limited to approximately 2-9 $Å^{-1}$) and the noticeable noise in the experimental data, the chemical identity and relative importance of possible contributions in the second shell cannot be identified unambiguously. This deduction is emphasized by the close agreement of the two fits depicted in Figure 2.

However, in general, the molecular structural data measured for Pu reacted with OPA are in accord for example with results obtained by Kersting et al. [57] for Pu interacting with several Fe/Mn minerals and alumina-silicates. For the Fe/Mn containing minerals goethite, birnessite, and pyrolusite an averaged Pu–O distance of 2.30 ± 0.01 Å (modelled by two sub-shells) with coordination numbers of 6-8 are reported. Further, a Pu-Fe/Mn second-shell contribution at R=3.33-3.43 Å was identified. For the alumina-silicates the mentioned study reports Pu–O coordination numbers of 8-10 and distances of 2.28-2.37 Å and a Si second-shell contribution at 3.11-3.14 Å.

Any additional scattering contributions at larger distances as typically observed for Pu precipitations or polynuclear species [36] cannot be detected in the EXAFS data (Figure 2). For further elaboration, an additional EXAFS data set is shown in Figure S1 depicting the spectroscopic results for Pu(IV) interaction with OPA. Despite the higher susceptibility to form precipitates or polynuclear species, no corresponding evidence is observed in the spectrum. However, similar to the spectrum shown in Figure 2, a distinct second shell contribution is detected. The absence of polynuclear species or secondary Pu precipitates, but the detection of second shell scattering pairs in the EXAFS spectroscopic data is indicative of inner-sphere sorption (covalent bonding) of Pu to surfaces of minerals present in the Opalinus Clay. However, due to the geochemical complexity of the OPA – in particular the

simultaneous presence of Fe/Mn minerals and alumina-silicates [41] – the predominant reactive phase(s) and immobilization process(es) cannot be further refined based on the present bulk measurements of a powder sample.

3.2 Spatially resolved investigations

3.2.1. OPA thin section sample

To develop a better understanding regarding the influence of geochemical complexity and (micro)heterogeneity on the local retention and chemical speciation of Pu in OPA, intact rock samples were examined with high spatial resolution. Multimodal microscopic chemical imaging and spatially resolved spectroscopy are employed to detect a possible variety of Pu species and to identify the reactive components of the OPA material. As a first type of intact rock samples, Figure 3 shows a thin section of OPA at different magnifications and probed with different microscopic tools. Figure 3a depicts a representative photograph of the OPA thin section. On this macroscopic scale the material appears to be rather homogeneous. However, already a moderately magnified view provided by visible light microcopy (Figure 3b) reveals a heterogeneous structure (see also e.g., [58, 59]). Increasing the spatial resolution further, microscopic chemical images obtained by X-ray microprobe analysis are shown in the two panels below in Figure 3 (c-g and h-l, respectively). Each of the two rows represents chemical information for a 120 x 120 μm^2 area. The two areas are separated by 500 µm as schematically sketched by the red squares in Figure 3b. Both sets of chemical images reveal a characteristic micro-scale geochemical heterogeneity comparable to earlier evidences [60-62]. Following the exposure of the intact thin section to a Millipore water (pH adjusted to 7.6) spiked with Pu(VI), the resulting Pu retention pattern after reaction are far from homogeneous (Figure 3g and l). Pronounced differences in the local reactivity of the OPA rock material regarding the local retention of Pu can be observed. Two types of hierarchical pattern are

recognized. First, with a characteristic length scale of hundred(s) of micrometers, larger domains with elevated local Pu concentrations are surrounded by areas in which only lowest plutonium concentrations are measured ('patch pattern'). Corresponding boundaries are indicated by the white dashed lines in Figure 3 (g, l). Second, within the Pu-rich patches, the local Pu concentration reveals a characteristic 'speckle pattern'. Local Pu hot spots with an extension of less than ~10 µm are observed. Accordingly, large concentration gradients are expressed. Within a few micrometers, the local Pu concentration is changing by more than two orders of magnitude.

Comparing the observed distribution pattern of Pu to the elemental maps of the geochemical indicator elements Ca, Ti, Mn, or Fe, no unequivocal correlation can be established. The recorded elemental maps do not provide obvious reference towards the reactive phase(s) being involved in the immobilization processes of Pu in OPA.

To further detail the variability of chemical speciation and oxidation states of Pu immobilized at the OPA surfaces, micro-XANES measurements were performed on several Pu hot spots. As an example, Figure 1 (middle) shows the Pu L_{III}-edge micro-XANES spectrum of a selected hot spot in the thin section sample (see Figure 3g; marked by circle). The Pu L_{III}-edge peak energy occurs at 18068 ± 1 eV, which is indicative of Pu being present predominantly in a +IV oxidation state [56]. The fractions of different Pu oxidation states in this particular hot spot were determined by LCFA to be 80 ± 3 % Pu(IV) and 20 ± 4 % Pu(V), respectively. Similar results were obtained for several other hot spots investigated on this sample.

The observed reduction from Pu(V, VI) to Pu(IV) requires at least one redox active electron donor couple (such as Fe^{2+}/Fe^{3+} or Mn^{2+}/Mn^{3+}) to be present in the OPA material. For various iron- and/or manganese (hydr-)oxide phases the (surface mediated) reduction of Pu and

subsequent immobilization of the newly formed reduced Pu species by immediate adsorption to the reducing phase have been postulated, with a limited number of studies providing direct spectroscopic evidence [26, 27, 57, 63]. In these studies, the covalent bonding of Pu to the Fe/Mn-mineral surfaces is evidenced by the observation of a second shell contribution in the EXAFS spectra best fitted with a Pu-Mn/Fe scattering path. Such a mechanism would result in a superposed spatial occurrence of Pu with the Fe/Mn-bearing phase as Pu is proposed to be immobilized directly on the surface of the grains acting as electron donor. The expected pronounced spatial correlation between Pu and Fe or Pu and Mn, however, was not observed in the present system (Figure 3). Based on the same argumentation, the proposed uptake of Pu species by calcite [28] can be rejected to be the predominant process of Pu immobilization. The local Pu concentrations show no evident correlation with the calcium distribution.

To obtain further information related to the mineral phases responsible for the reduction and retention of Pu in the present experiment, selected areas including Pu hot spots were analyzed by combined two-dimensional micro-XRF and micro-XRD chemical imaging. First of all, despite a scattering volume as low as ~100 μm^3, the individual two-dimensional XRD pattern recorded in each pixel exhibit a pronounced complexity (Figure S2) reflecting the mineralogical micro-/nano-heterogeneity and intricacy of the OPA material. Nevertheless, comparing the average XRD pattern obtained for pixels with higher Pu local concentrations to the average XRD pattern observed at lower local Pu levels reveals one noticeable difference. Pixels with elevated Pu show increased intensities of a few selected reflections, which all can be assigned to kaolinite (001, 002, 003, 004 reflections; Figure S2). The spatial correlation of the local Pu concentration and the kaolinite distribution can be demonstrated by micro-XRF/XRD chemical imaging, as shown in Figure 4. The top panel depicts an image of the local distribution of Pu (see related yellow square in Figure 3l), the corresponding zoom-in (11 x 11 μm^2 area) is depicted in the top left of the main panel of Figure 4. Below, the related

456 spatial distributions of the mineral phases kaolinite and illite are shown. The similarity of the
457 Pu and kaolinite distribution is readily apparent. Opposite, Pu and illite (another clay mineral
458 phase commonly considered as highly reactive in OPA [21, 64-66]) show a pronounced anti-
459 correlation. Similarly, Fe, Mn, Ca (depicted in the right column of the main panel of Figure 4)
460 and additional trace elements are not present in the location of immobilization of Pu.
461
462 The correlation between the local concentrations of Pu and local kaolinite content is shown in
463 Figure S3. A clear positive correlation can be deduced. One has even to recognize that several
464 experimental parameters or boundary conditions contribute to an easing of an existing
465 correlation. First of all, in case of processes occurring at the mineral-solution interface being
466 the dominant immobilization mechanism (such as adsorption or surface mediated secondary
467 phase precipitation), the ratio of Pu XRF versus kaolinite XRD intensities is related to the
468 local specific surface area of the kaolinite grains. Second, despite simultaneous data
469 collection, the 'response' voxels for XRD and XRF are not identical. This is further amplified
470 by the limited equilibration time of only 5 days resulting in enhanced Pu reactivity at the
471 solution-side surface of the thin section, while XRD probes along the entire thickness of the
472 thin section. Additional disturbances are caused by the established preferential orientation of
473 the platelets in the kaolinite domains (Figure S2). OPA is known to be an anisotropic
474 sedimentary rock [67]. Depending on the spatial alignment, certain kaolinite platelets are 'not
475 visible' in the XRD measurements, while the related XRF based detection of the Pu
476 concentration is not effected by the anisotropic nature of the porous medium. Despite these
477 constraints, a convincing relation between Pu immobilization and local kaolinite appearance
478 can be established. Consequently, the final immobilization of Pu is either directly related to
479 kaolinite as reactive sorbent or to a geochemically linked (possibly highly disordered, X-ray
480 amorphous) phase.
481

While kaolinite turns out to be involved in the final immobilization process, kaolinite cannot be expected to be responsible for the spectroscopically confirmed reduction of Pu(V,VI) to Pu(IV) prior to adsorption. Consequently, the reduction and the retardation do not occur as combined process on a single reactive surface. The immobilization of Pu(V,VI) in Opalinus Clay has to be represented by a multi-step mechanism with the two fundamental processes (i) reduction and (ii) sorption as two decoupled, subsequent, and spatially separated processes involving different reactive phases of the Opalinus Clay rock. First, the Fe(II)-bearing minerals siderite and pyrite present in significant quantities in Opalinus Clay possibly act as the redox active mineral phases. Evidence for the presence of siderite in the vicinity of the Pu hotspots is indeed provided by the micro-XRD imaging (Figure S2c). Second, kaolinite or a geochemically related phase present in the vicinity of the Fe(II)-bearing phase expresses the highest reactivity towards the sorption of the reduced Pu(IV).

An additional piece of evidence is provided by spectroscopic results obtained after sorption of reduced Pu(IV) to OPA powder (EXAFS data shown in Figure S1). This approach allows an isolated experimental investigation of the proposed second step, the immobilization of the reduced Pu(IV) by a reactive compound of OPA. The distinct second shell contribution can be fitted by a Pu-Al/Si second shell as one would expect for Pu sorbed to kaolinite. No additional, heaver backscatterer (such as, e.g., Fe) are required to obtain a satisfactory fit.

3.2.2. OPA core diffusion sample

To investigate sorption and diffusion processes under even more realistic conditions, Pu(V,VI) in-diffusion into OPA was examined experimentally. After an extended period of time (30 days), the Pu distribution and speciation at the surface of the OPA piece in contact with the Pu spiked reservoir solution were investigated.

Microscopic chemical images depicting the Pu distribution in relation to geochemical indicator elements such as Ca, Ti, Mn, or Fe are presented in Figure S4. The observed characteristic of the distribution pattern and the elemental correlations are analogous to the pattern observed and discussed for the thin section experiment (Figure 3).

Several spots of higher Pu concentration were analyzed by micro-XANES. A representative Pu L_{III}-edge micro-XANES spectrum (Figure 1, bottom) shows that Pu(IV) is the dominating oxidation state (70 ± 3 %). Only minor fractions of initial Pu(V) of about 22 ± 5 % and Pu(VI) close to the detection limit (8 ± 6 %) are observed. The Pu(V,VI) in-diffusion into a bulk clay rock piece - investigated at the reservoir-rock interface - yields results in agreement with the other two types of investigations discussed before.

4. Environmental implications

The three different complementary types of investigations of this study yield coherent information relevant to the migration of Pu in engineered barrier systems and related geological subsurface systems. First, in all systems the Pu introduced as Pu(V,VI) was reduced by redox active components of the Opalinus Clay, to Pu(IV) with a smaller/minority fraction remaining as Pu(V). Chemical imaging shows the reduced Pu to be immobilized in the vicinity of the potentially redox active elements Fe and Mn. However, high resolution microscopic chemical imaging based on micro-XRF reveals unambiguously that the domains with immobilized Pu show only lowest local concentrations of Fe, Mn, Ti, or Ca. The domains reactive in terms of Pu immobilization are dominated by elements not detectable by the employed micro-XRF imaging configuration, in particular Al and Si. Accordingly, several geochemically reactive phases proposed in the context of surface mediated reduction and adsorption of Pu such as Mn(II) or Fe(II)-bearing oxides [24, 25, 27], or calcite [28] can be rejected

as the reactive adsorption components (sorbents) in OPA under the conditions investigated in the present study. Further, possible secondary Pu phase precipitation (with high crystallinity) can be ruled out based on the EXAFS results. Consequently, in the present system Pu immobilization has to be based on a reactive process occurring at the pore water–rock interface such as adsorption to an Al/Si phase or the incorporation of Pu into a newly formed poorly crystalline (X-ray amorphous) Al/Si phase. This proposition is supported by the observed 2nd shell scattering contributions in the EXAFS data. Additional evidence is provided by combined micro-XRF/micro-XRD chemical imaging results revealing that the clay mineral kaolinite is consistently observed within the reactive micro-domains of high Pu retention. Opposite, no crystallographic evidence was found at these locations of high Pu concentration for enhanced localized availability of plausible electron donors, in particular Fe(II)-bearing mineral phases such as siderite or pyrite. This combination of findings provides strong evidence that at least two reactive components have to be involved in the observed 'reductive immobilization' of Pu in OPA. The electron donor and the immobilizing sorbent are two distinct, spatially separated components. Geological phases such as siderite or pyrite act as electron donor pools and buffer the redox potential locally, while a second OPA component exhibits a high sorption affinity for the reduced Pu(IV) species and acts as a strong sink affecting the stability field for the sorbed Pu(IV) compared to the aqueous species [20].

Natural geological and engineered barrier materials are commonly complex and heterogeneous. In-situ multimodal microscopic studies under conditions relevant to deep geological formations are crucial to identify the reactive components and reaction pathways or to validate proposed mechanisms. The present study demonstrated that a simplistic description by a sole reactive component is not an adequate representation of the geochemical reactivity responsible for the immobilization of Pu(V,VI) within an Opalinus Clay barrier.

Studies on intact, undisturbed systems are absolutely essential to ascertain the geochemical reactivity for relevant geochemical conditions and settings.

In addition to providing essential information related to the safety assessment of nuclear waste disposal concepts, the presented observations contribute to advance our understanding of (redox-sensitive) radionuclide transport in the geosphere in general. Based on the employed chemical imaging, further progress can be expected by representing reactive transport even dynamically by a series of subsequent patterns.

Acknowledgments

This work was financed by the German Federal Ministry for Economic Affairs and Energy (BMWi) under contract No. 02E10166 and the European Commission under the 7th Framework Programme: ACTINET-I3 (Grant no. 232631). We acknowledge the ESRF for provision of synchrotron beam time and thank Andreas Scheinost, Christoph Hennig, and Dipanian Banerjee from the Helmholtz-Zentrum Dresden-Rossendorf, Germany, for the experimental support during the XAS measurements at ROBL. Microscopic chemical imaging and microspectroscopic measurements were performed at the microXAS beamline of the Swiss Light Source (SLS), Paul Scherrer Institute, Switzerland. We acknowledge the PSI/SLS for provision of synchrotron beam time, handling of the radioactive samples at the PSI hot laboratory, and excellent user support during the microprobe measurements. We acknowledge the support of Daniel Fröhlich (Institute of Nuclear Chemistry, Johannes Gutenberg-Universität Mainz, Germany during the experiments. We are grateful to Christian Marquardt

580 (Institute for Nuclear Waste Disposal, Karlsruher Institut für Technologie) for providing the
581 OPA samples. Maik Biegler (Max-Planck-Institut für Chemie, Mainz) is acknowledged for
582 preparation of the thin sections. Reference spectra of Pu(IV), and Pu(V) have been kindly
583 provided by Philipe Martin, CEA, France, and Christophe Den Auwer, Université de Nice
584 Sophia Antipolis, France, respectively.

585

586

587

588

589 **Supporting Information**

590 Additional experimental details and supplementary results (PDF)

591

592

593

594

595 **Figure Captions**

596

597 **Figure 1**:

598 Normalized Pu L_{III}-edge XANES spectra of Pu(VI) interacted with different samples of
599 Opalinus Clay rock material. top) OPA powder sample; middle) OPA thin section; bottom)
600 OPA core diffusion sample. In each panel experimental data are compared to corresponding
601 linear combination fits of Pu(III)[50], Pu(IV)[51], Pu(V)[52], and Pu(VI)[53]). Contributions of
602 individual components are included in the figures.

603

604 **Figure 2:**

605 Pu L_{III}-edge k^3-weighted EXAFS spectrum (left) and corresponding Fourier transform
606 magnitude (right) of Pu(VI) interacted with Opalinus Clay powder. Experimental data are
607 compared to two different two-shell fits consisting of a first Pu-O shell and the second shells
608 correspond to different combinations of Pu-Si/Al and Pu-Fe/Mn backscattering pairs. The
609 green line corresponds to a fit obtained using a combination of Pu-Si/Al and Pu-Fe/Mn
610 scattering pairs in the second coordination shell, while the red line is based on two distinct
611 sub-shells considering only Si/Al in the second shell (Table S4).

612

613 **Figure 3:**

614 Sorption experiment of a Opalinus Clay thin section sample reacting with Pu spiked Millipore
615 water. a) photograph of a representative thin section, b) corresponding light microscope
616 image, c-g) and h-l) elemental distributions of Ca, Ti, Mn, Fe, and Pu for two areas. Chemical
617 images were obtained by synchrotron-based micro-XRF. A pronounced geochemical
618 heterogeneity is observed on the micron-scale.
619 The rectangles sketch magnified zoom-in areas depicted in subsequent panels. The yellow
620 circle in top-left corner of Figure 3g) indicates the location of the micro-XANES
621 measurement shown in Figure 1 (middle).

622

623 **Figure 4:**

624 Multi-modal microscopic imaging of a domain with high local Pu retardation observed within
625 the Opalinus Clay thin section. Elemental distribution maps of Pu, Fe, Mn, and Ca were
626 recorded by micro-XRF while mineral distributions of illite and kaolinite are based on micro-
627 XRD imaging.

REFERENCES

1. NEA/AEN, Features, Events and Processes (FEPs) for Geologic Disposal of Radioactive Waste - An International Database. Paris, 2000.
2. NAGRA, FEP Management for Safety Assessment (Project Opalinus Clay). Nagra Technical Report NTB-02-23, NAGRA Nationale Genossenschaft für die Lagerung radioaktiver Abfälle, Wettingen, Switzerland, 2002.
3. Gompper, K., Zur Abtrennung langlebiger Radionuklide. Forschungszentrum Karlsruhe: Karlsruhe, 2000.
4. ONDRAF/NIRAS, Technical overview of the SAFIR 2 report, Technical Report NIROND 2001. ONDRAF, Brussels, 2001.
5. OECD, Safety of geological disposal of high-level and long-lived radioactive waste in France - An international peer review of the "Dossier 2005 Argile" concerning disposal in the Callovo - Oxfordian formation. Organisation for Economic Co-operation and Development, Paris, 2006.
6. Hoth, P.; Wirth, H.; Reinhold, K.; Bräuer, V.; Krull, P.; Feldrappe, H., Endlagerung radioaktiver Abfälle in tiefen geologischen Formationen Deutschlands – Untersuchung und Bewertung von Tongesteinsformationen. In Bundesanstalt für Geowissenschaften und Rohstoffe (BGR): Berlin/Hannover, 2007.
7. NAGRA, Project Opalinus Clay: Safety Report – Demonstration of disposal feasibility for spent fuel, vitrified high-level waste and long-lived intermediate-level waste (Entsorgungsnachweis). Nagra Technical Report NTB-02-05, NAGRA Nationale Genossenschaft für die Lagerung radioaktiver Abfälle, Wettingen, Switzerland, 2002.
8. Lemire, R.; Fuger, J.; Nitsche, H.; Potter, P.; Rand, M. H.; Rydberg, J.; Spahiu, K.; Sullivan, J. C.; Ullman, W. J.; Vitorge, P.; Warner, H., Chemical Thermodynamics of Neptunium and Plutonium. Elsevier: Amsterdam, 2001.
9. Neck, V.; Altmaier, M.; Fanghanel, T., Solubility of plutonium hydroxides/hydrous oxides under reducing conditions and in the presence of oxygen. C. R. Chim. 2007, 10, (10-11), 959-977.
10. Runde, W., The chemical interactions of actinides in the environment. Los Alamos Science 2000, 26, 392-411.
11. Choppin, G. R., Actinide speciation in the environment. J. Radioanal. Nucl. Chem. 2007, 273, (3), 695-703.
12. Runde, W.; Conradson, S. D.; Efurd, D. W.; Lu, N. P.; VanPelt, C. E.; Tait, C. D., Solubility and sorption of redox-sensitive radionuclides (Np, Pu) in J-13 water from the Yucca Mountain site: comparison between experiment and theory. Appl. Geochem. 2002, 17, (6), 837-853.
13. Kaplan, D. I.; Powell, B. A.; Demirkanli, D. I.; Fjeld, R. A.; Molz, F. J.; Serkiz, S. M.; Coates, J. T., Influence of oxidation states on plutonium mobility during long-term transport through an unsaturated subsurface environment. Environ. Sci. Technol. 2004, 38, (19), 5053-5058.
14. NAGRA, Geologische Tiefenlagerung der abgebrannten Brennelemente, der hochaktiven und langlebigen mittelaktiven Abfälle — Darstellung und Beurteilung der aus sicherheitstechnisch-geologischer Sicht möglichen Wirtsgesteine und Gebiete. Nagra Technical Report NTB-05-02, NAGRA Nationale Genossenschaft für die Lagerung radioaktiver Abfälle, Wettingen, Switzerland, 2005.

15. Mazurek, M.; Alt-Epping, P.; Bath, A.; Gimmi, T.; Waber, H. N.; Buschaert, S.; De Canniere, P.; De Craen, M.; Gautschi, A.; Savoye, S.; Vinsot, A.; Wemaere, I.; Wouters, L., Natural tracer profiles across argillaceous formations. Appl. Geochem. 2011, 26, (7), 1035-1064.
16. Appelo, C. A. J.; Van Loon, L. R.; Wersin, P., Multicomponent diffusion of a suite of tracers (HTO, Cl, Br, I, Na, Sr, Cs) in a single sample of Opalinus Clay. Geochim. Cosmochim. Acta 2010, 74, (4), 1201-1219.
17. Missana, T.; Alonso, U.; Garcia-Gutierrez, M.; Mingarro, M., Role of bentonite colloids on europium and plutonium migration in a granite fracture. Appl. Geochem. 2008, 23, (6), 1484-1497.
18. Kersting, A. B.; Efurd, D. W.; Finnegant, D. L.; Rokop, D. J.; Smith, D. K.; Thompson, J. L., Migration of Plutonium in Ground Water at the Nevada Test Site. Nature 1999, 397, 56-59.
19. Buda, R. A.; Banik, N. L.; Kratz, J. V.; Trautmann, N., Studies of the ternary systems humic substances - kaolinite - Pu(III) and Pu(IV). Radiochim. Acta 2008, 96, (9-11), 657-665.
20. Marsac, R.; Banik, N. L.; Lutzenkirchen, J.; Buda, R. A.; Kratz, J. V.; Marquardt, C. M., Modeling plutonium sorption to kaolinite: Accounting for redox equilibria and the stability of surface species. Chem. Geol. 2015, 400, 1-10.
21. Banik, N. L.; Marsac, R.; Lutzenkirchen, J.; Diascorn, A.; Bender, K.; Marquardt, C. M.; Geckeis, H., Sorption and Redox Speciation of Plutonium at the Illite Surface. Environ. Sci. Technol. 2016, 50, (4), 2092-2098.
22. Zavarin, M.; Powell, B. A.; Bourbin, M.; Zhao, P. H.; Kersting, A. B., Np(V) and Pu(V) Ion Exchange and Surface-Mediated Reduction Mechanisms on Montmorillonite. Environ. Sci. Technol. 2012, 46, (5), 2692-2698.
23. Begg, J. D.; Zavarin, M.; Zhao, P. H.; Tumey, S. J.; Powell, B.; Kersting, A. B., Pu(V) and Pu(IV) Sorption to Montmorillonite. Environ. Sci. Technol. 2013, 47, (10), 5146-5153.
24. Sanchez, A. L.; Murray, J. W.; Sibley, T. H., The absorption of plutonium(IV) and plutonium(V) on goethite. Geochim. Cosmochim. Acta 1985, 49, (11), 2297-2307.
25. Powell, B. A.; Fjeld, R. A.; Kaplan, D. I.; Coates, J. T.; Serkiz, S. M., PU(V)0(2)(+) adsorption and reduction by synthetic hematite and goethite. Environ. Sci. Technol. 2005, 39, (7), 2107-2114.
26. Shaughnessy, D. A.; Nitsche, H.; Booth, C. H.; Shuh, D. K.; Waychunas, G. A.; Wilson, R. E.; Gill, H.; Cantrell, K. J.; Serne, R. J., Molecular interfacial reactions between Pu(VI) and manganese oxide minerals manganite and hausmannite. Environ. Sci. Technol. 2003, 37, (15), 3367-3374.
27. Kirsch, R.; Fellhauer, D.; Altmaier, M.; Neck, V.; Rossberg, A.; Fanghanel, T.; Charlet, L.; Scheinost, A. C., Oxidation State and Local Structure of Plutonium Reacted with Magnetite, Mackinawite, and Chukanovite. Environ. Sci. Technol. 2011, 45, (17), 7267-7274.
28. Zavarin, M.; Roberts, S. K.; Hakem, N.; Sawvel, A. M.; Kersting, A. B., Eu(III), Sm(III), Np(V), Pu(V), and Pu(IV) sokption to calcite. Radiochim. Acta 2005, 93, (2), 93-102.
29. Amayri, S.; Frohlich, D. R.; Kaplan, U.; Trautmann, N.; Reich, T., Distribution coefficients for the sorption of Th, U, Np, Pu, and Am on Opalinus Clay. Radiochim. Acta 2016, 104, (1), 33-40.
30. Begg, J. D.; Zavarin, M.; Tumey, S. J.; Kersting, A. B., Plutonium sorption and desorption behavior on bentonite. Journal of Environmental Radioactivity 2015, 141, 106-114.

31. Hixon, A. E.; Hu, Y. J.; Kaplan, D. I.; Kukkadapu, R. K.; Nitsche, H.; Qafoku, O.; Powell, B. A., Influence of iron redox transformations on plutonium sorption to sediments. Radiochim. Acta 2010, 98, (9-11), 685-692.
32. Kersting, A. B., Plutonium Transport in the Environment. Inorg. Chem. 2013, 52, (7), 3533-3546.
33. Ashida, T.; Kohara, Y.; Yui, M., Migration behavior of Pu released from Pu-doped glass in compacted bentonite. Radiochim. Acta 1994, 66-7, 359-362.
34. Kaplan, D. I.; Powell, B. A.; Duff, M. C.; Demirkanli, D. I.; Denham, M.; Fjeld, R. A.; Molz, F. J., Influence of sources on plutonium mobility and oxidation state transformations in vadose zone sediments. Environ. Sci. Technol. 2007, 41, (21), 7417-7423.
35. Powell, B. A.; Kaplan, D. I.; Serkiz, S. M.; Coates, J. T.; Fjeld, R. A., Pu(V) transport through Savannah River Site soils - an evaluation of a conceptual model of surface-mediated reduction to Pu (IV). Journal of Environmental Radioactivity 2014, 131, 47-56.
36. Reich, T.; Reich, T. Y.; Amayri, S.; Drebert, J.; Banik, N. L.; Buda, R. A.; Kratz, J. V.; Trautmann, N., Application of XAFS spectroscopy to actinide environmental science. In X-Ray Absorption Fine Structure-XAFS13, Hedman, B.; Painetta, P., Eds. Amer Inst Physics: Melville, 2007; Vol. 882, pp 179-183.
37. Duff, M. C.; Hunter, D. B.; Triay, I. R.; Bertsch, P. M.; Reed, D. T.; Sutton, S. R.; Shea-Mccarthy, G.; Kitten, J.; Eng, P.; Chipera, S. J.; Vaniman, D. T., Mineral associations and average oxidation states of sorbed Pu on tuff. Environ. Sci. Technol. 1999, 33, (13), 2163-2169.
38. Duff, M. C.; Hunter, D. B.; Triay, I. R.; Bertsch, P. M.; Kitten, J.; Vaniman, D. T., Comparison of two micro-analytical methods for detecting the spatial distribution of sorbed Pu on geologic materials. J. Contam. Hydrol. 2001, 47, (2-4), 211-218.
39. Denecke, M. A.; Somogyi, A.; Janssens, K.; Simon, R.; Dardenne, K.; Noseck, U., Microanalysis (micro-XRF, micro-XANES, and micro-XRD) of a tertiary sediment using microfocused synchrotron radiation. Microsc. Microanal. 2007, 13, (3), 165-172.
40. Frohlich, D. R.; Amayri, S.; Drebert, J.; Grolimund, D.; Huth, J.; Kaplan, U.; Krause, J.; Reich, T., Speciation of Np(V) uptake by Opalinus Clay using synchrotron microbeam techniques. Analytical and Bioanalytical Chemistry 2012, 404, (8), 2151-2162.
41. Pearson, F. J.; Arcos, D.; Bath, A.; Boisson, J.-Y.; Fernández, A. M.; Gäbler, H.-E.; Gaucher, E.; Gautschi, A.; Griffault, L.; Hernán, P.; Waber, H. N. Mont Terri Project - Geochemistry of water in the opalinus clay formation at the Mont Terri rock laboratory. BWGG-5-E, Reports of the FOWG. Geology series; Federal Office for the Environment FOEN, Bern, 2003.
42. Wu, T.; Amayri, S.; Drebert, J.; Van Loon, L. R.; Reich, T., Neptunium(V) Sorption and Diffusion in Opalinus Clay. Environ. Sci. Technol. 2009, 43, (17), 6567-6571.
43. Van Loon, L. R.; Soler, J. M.; Jakob, A.; Bradbury, M. H., Effect of confining pressure on the diffusion of HTO, $^{36}Cl^-$ and $^{125}I^-$ in a layered argillaceous rock (Opalinus Clay): diffusion perpendicular to the fabric. Appl. Geochem. 2003, 18, (10), 1653-1662.
44. Joseph, C.; Van Loon, L. R.; Jakob, A.; Steudtner, R.; Schmeide, K.; Sachs, S.; Bernhard, G., Diffusion of U(VI) in Opalinus Clay: Influence of temperature and humic acid. Geochim. Cosmochim. Acta 2013, 109, 74-89.
45. Matz, W.; Schell, N.; Bernhard, G.; Prokert, F.; Reich, T.; Claussner, J.; Oehme, W.; Schlenk, R.; Dienel, S.; Funke, H.; Eichhorn, F.; Betzl, M.; Prohl, D.; Strauch, U.; Huttig, G.; Krug, H.; Neumann, W.; Brendler, V.; Reichel, P.; Denecke, M. A.; Nitsche, H., ROBL - a CRG beamline for radiochemistry and materials research at the ESRF. Journal of Synchrotron Radiation 1999, 6, 1076-1085.

46. Ravel, B.; Newville, M., ATHENA, ARTEMIS, HEPHAESTUS: data analysis for X-ray absorption spectroscopy using IFEFFIT. Journal of Synchrotron Radiation 2005, 12, 537-541.
47. George, G. N.; Pickering, I. J. EXAFSPAK: A Suite of Computer Programs for the Analysis of X-ray Absorption Spectra, Stanford Synchrotron Radiation Laboratory.: Stanford, 1995.
48. Ankudinov, A. L.; Bouldin, C. E.; Rehr, J. J.; Sims, J.; Hung, H., Parallel calculation of electron multiple scattering using Lanczos algorithms. Phys. Rev. B 2002, 65, (10), 11.
49. Albering, J. H.; Jeitschko, W., The crystal structures of $Th_4Fe17P_{10}O_{1-X}$ and $ThFe_5P_3$. J. Solid State Chem. 1995, 117, (1), 80-87.
50. Schmeide, K.; Reich, T.; Sachs, S.; Bernhard, G., Plutonium(III) complexation by humic substances studied by X-ray absorption fine structure spectroscopy. Inorg. Chim. Acta 2006, 359, (1), 237-242.
51. Martin, P.; Grandjean, S.; Valot, C.; Carlot, G.; Ripert, M.; Blanc, P.; Hennig, C., XAS study of $(U_{1-y}Pu_y)O_2$ solid solutions. Journal of Alloys and Compounds 2007, 444–445, 410-414.
52. Di Giandomenico, M. V.; Le Naour, C.; Simoni, E.; Guillaumont, D.; Moisy, P.; Hennig, C.; Conradson, S. D.; Den Auwer, C., Structure of early actinides(V) in acidic solutions. Radiochim. Acta 2009, 97, (7), 347-353.
53. Reich, T.; Geipel, G.; Funke, H.; Hennig, C.; Rossberg, A.; Bernhard, G. Plutonium. XAFS measurements of plutonium hydrates, ESRF: Grenoble (F), 2000; pp 32-33.
54. De Nolf, W.; Vanmeert, F.; Janssens, K., XRDUA: crystalline phase distribution maps by two-dimensional scanning and tomographic (micro) X-ray powder diffraction. J. Appl. Crystallogr. 2014, 47, 1107-1117.
55. Conradson, S. D.; Abney, K. D.; Begg, B. D.; Brady, E. D.; Clark, D. L.; den Auwer, C.; Ding, M.; Dorhout, P. K.; Espinosa-Faller, F. J.; Gordon, P. L.; Haire, R. G.; Hess, N. J.; Hess, R. F.; Keogh, D. W.; Lander, G. H.; Lupinetti, A. J.; Morales, L. A.; Neu, M. P.; Palmer, P. D.; Paviet-Hartmann, P.; Reilly, S. D.; Runde, W. H.; Tait, C. D.; Veirs, D. K.; Wastin, F., Higher order speciation effects on plutonium L-3 X-ray absorption near edge spectra. Inorg. Chem. 2004, 43, (1), 116-131.
56. Conradson, S. D.; Al Mahamid, I.; Clark, D. L.; Hess, N. J.; Hudson, E. A.; Neu, M. P.; Palmer, P. D.; Runde, W. H.; Tait, C. D., Oxidation state determination of plutonium aquo ions using x-ray absorption spectroscopy. Polyhedron 1998, 17, (4), 599-602.
57. Kersting, A. B.; Zhao, P.; Zavarin, M.; Sylwester, E. R.; Allen, P. G.; Williams, R. W., Sorption of Pu(V) on mineral colloids. . In Colloidal-Facilitated Transport of Low-Solubility Radionuclides: A Field, Experimental, and Modeling Investigation, A.B., K.; Remus, P. W., Eds. Lawrence Livermore National Laboratory Livermore, CA, USA, Vol. Report UCRL-ID-149688.
58. Houben, M. E.; Desbois, G.; Urai, J. L., A comparative study of representative 2D microstructures in Shaly and Sandy facies of Opalinus Clay (Mont Terri, Switzerland) inferred form BIB-SEM and MIP methods. Marine and Petroleum Geology 2014, 49, 143-161.
59. Marschall, P.; Horseman, S.; Gimmi, T., Characterisation of gas transport properties of the Opalinus clay, a potential host rock formation for radioactive waste disposal. Oil Gas Sci. Technol. 2005, 60, (1), 121-139.
60. Wang, H. A. O.; Grolimund, D.; Van Loon, L. R.; Barmettler, K.; Borca, C. N.; Aeschimann, B.; Gunther, D., Quantitative Chemical Imaging of Element Diffusion into Heterogeneous Media Using Laser Ablation Inductively Coupled Plasma Mass Spectrometry, Synchrotron Micro-X-ray Fluorescence, and Extended X-ray Absorption Fine Structure Spectroscopy. Anal. Chem. 2011, 83, (16), 6259-6266.

825 61. Wang, H. A. O.; Grolimund, D.; Van Loon, L. R.; Barmettler, K.; Borca, C. N.;
826 Aeschlimann, B.; Gunther, D., High Spatial Resolution Quantitative Imaging by Cross-
827 calibration Using Laser Ablation Inductively Coupled Plasma Mass Spectrometry and
828 Synchrotron Micro-X-ray Fluorescence Technique. Chimia 2012, 66, (4), 223-228.
829 62. Grolimund, D.; Wang, H. A. O.; Van Loon, L. R.; Marone, F.; Diaz, N.; Kaestner, A.;
830 Jakob, A., Microscopic Chemical Imaging: A Key to Understand Ion Mobility in Tight
831 Formations. In CMS Workshop Lecture Series, Society, C. M., Ed. 2016; pp 1-24.
832 63. Hu, Y. J.; Schwaiger, L. K.; Booth, C. H.; Kukkadapu, R. K.; Cristiano, E.; Kaplan, D.;
833 Nitsche, H., Molecular interactions of plutonium(VI) with synthetic manganese-
834 substituted goethite. Radiochim. Acta 2010, 98, (9-11), 655-663.
835 64. Bradbury, M. H.; Baeyens, B., A generalised sorption model for the concentration
836 dependent uptake of caesium by argillaceous rocks. J. Contam. Hydrol. 2000, 42, (2-4),
837 141-163.
838 65. Bradbury, M. H.; Baeyens, B., Predictive sorption modelling of Ni(II), Co(II), Eu(IIII),
839 Th(IV) and U(VI) on MX-80 bentonite and Opalinus Clay: A "bottom-up" approach.
840 Appl. Clay Sci. 2011, 52, (1-2), 27-33.
841 66. Joseph, C.; Stockmann, M.; Schmeide, K.; Sachs, S.; Brendler, V.; Bernhard, G.,
842 Sorption of U(VI) onto Opalinus Clay: Effects of pH and humic acid. Appl. Geochem.
843 2013, 36, 104-117.
844 67. Salager, S.; Francois, B.; Nuth, M.; Laloui, L., Constitutive analysis of the mechanical
845 anisotropy of Opalinus Clay. Acta Geotech. 2013, 8, (2), 137-154.

846

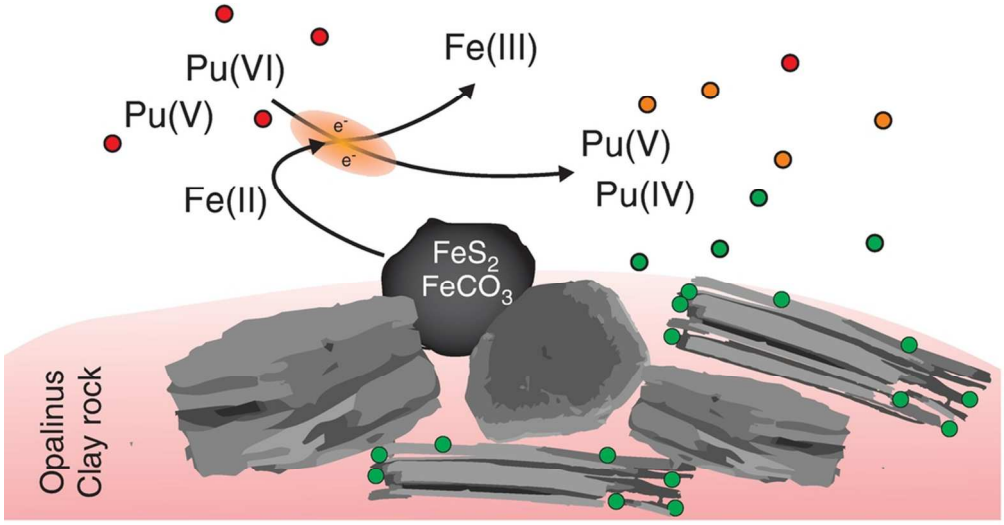

Reduction of Pu(VI), Pu(V) and immobilization of Pu(IV) in Opalinus Clay

TOC entry

91x59mm (300 x 300 DPI)

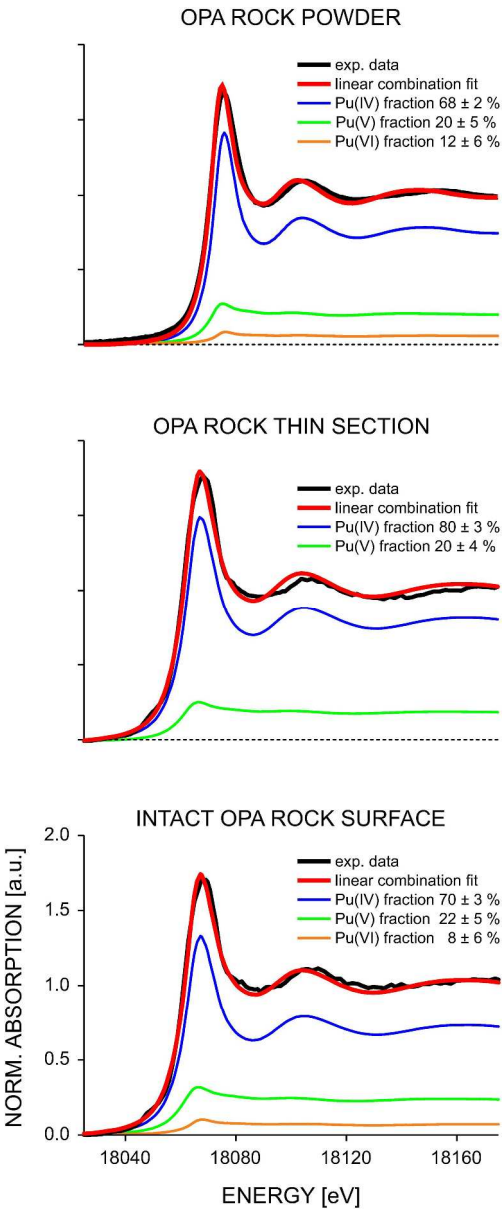

Normalized Pu LIII-edge XANES spectra of Pu(VI) interacted with different samples of Opalinus Clay rock material. top) OPA powder sample; middle) OPA thin section; bottom) OPA core diffusion sample. In each panel experimental data are compared to corresponding linear combination fits of Pu(III)50, Pu(IV)51, Pu(V)52, and Pu(VI)53). Contributions of individual components are included in the figures.

228x552mm (300 x 300 DPI)

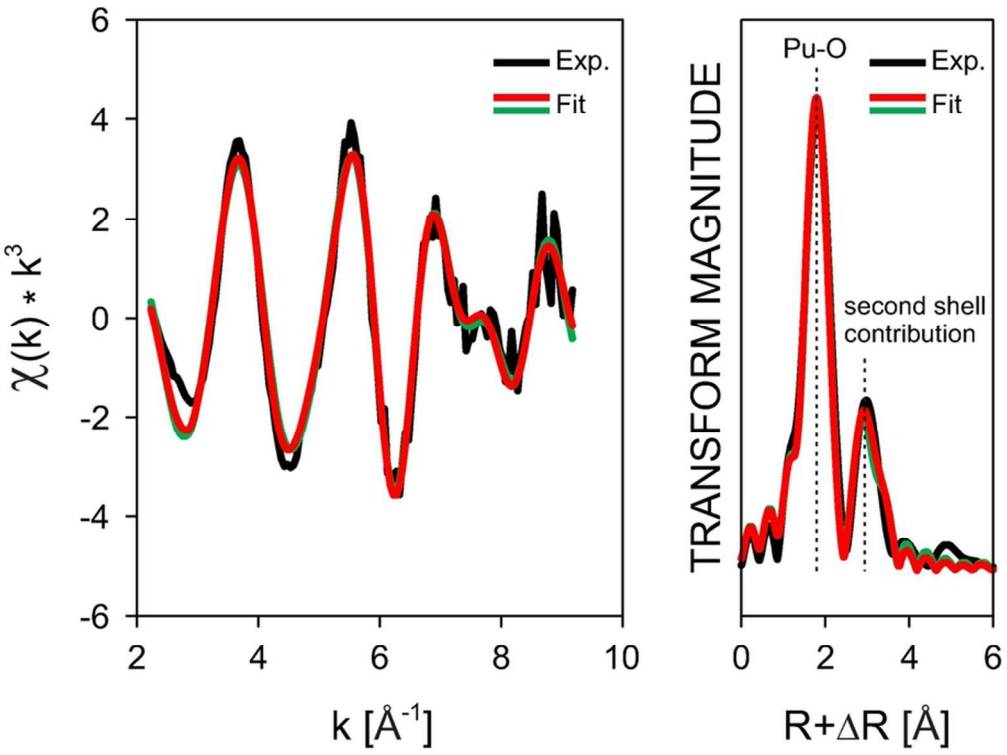

Pu LIII-edge k3-weighted EXAFS spectrum (left) and corresponding Fourier transform magnitude (right) of Pu(VI) interacted with Opalinus Clay powder. Experimental data are compared to two different two-shell fits consisting of a first Pu-O shell and the second shells correspond to different combinations of Pu-Si/Al and Pu-Fe/Mn backscattering pairs. The green line corresponds to a fit obtained using a combination of Pu-Si/Al and Pu-Fe/Mn scattering pairs in the second coordination shell, while the red line is based on two distinct sub-shells considering only Si/Al in the second shell (Table S4).

77x57mm (300 x 300 DPI)

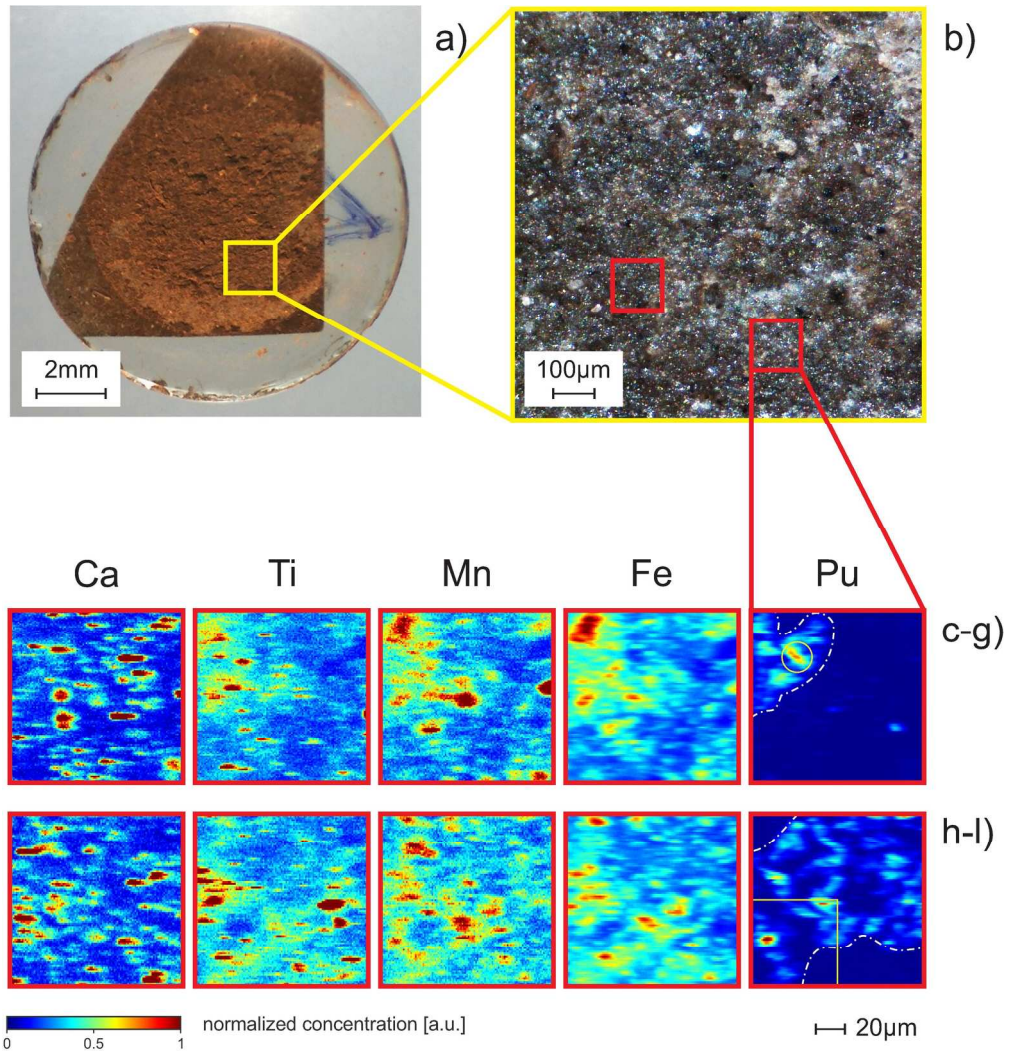

Sorption experiment of a Opalinus Clay thin section sample reacting with Pu spiked Millipore water. a) photograph of a representative thin section, b) corresponding light microscope image, c-g) and h-l) elemental distributions of Ca, Ti, Mn, Fe, and Pu for two areas. Chemical images were obtained by synchrotron-based micro-XRF. A pronounced geochemical heterogeneity is observed on the micron-scale. The rectangles sketch magnified zoom-in areas depicted in subsequent panels. The yellow circle in top-left corner of Figure 3g) indicates the location of the micro-XANES measurement shown in Figure 1 (middle).

181x189mm (300 x 300 DPI)

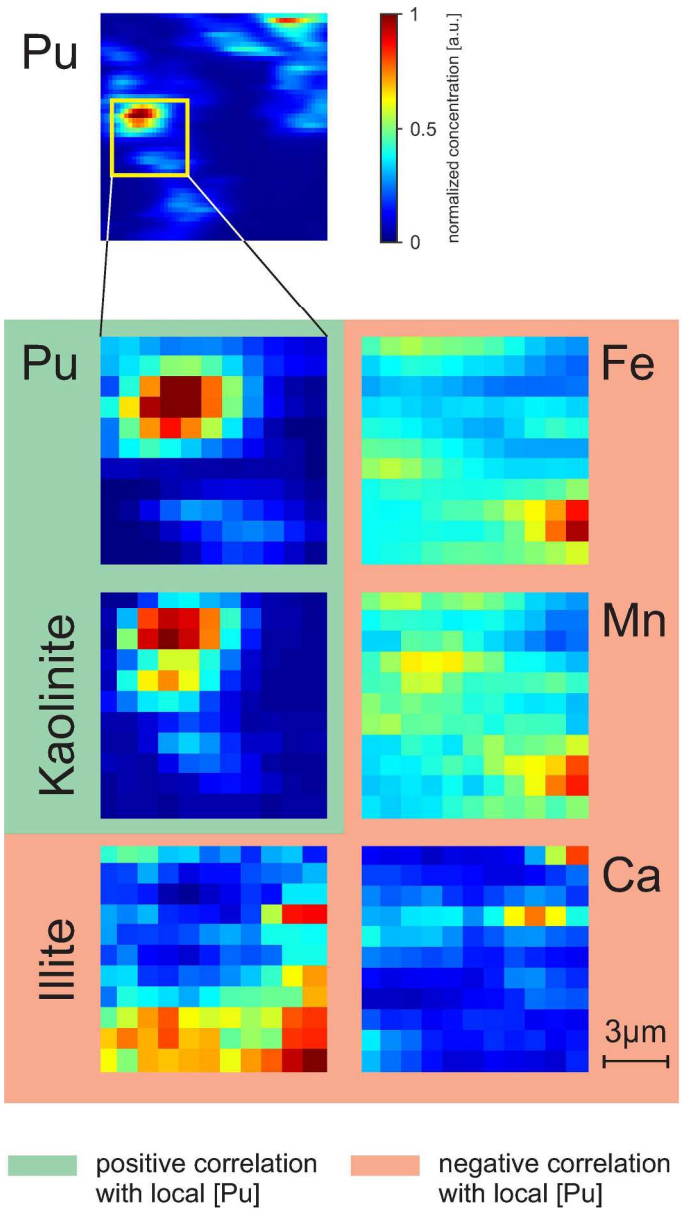

Multi-modal microscopic imaging of a domain with high local Pu retardation observed within the Opalinus Clay thin section. Elemental distribution maps of Pu, Fe, Mn, and Ca were recorded by micro-XRF while mineral distributions of illite and kaolinite are based on micro-XRD imaging.

158x281mm (300 x 300 DPI)